Soil Dynamics and Earthquake Engineering, 2019, Vol. 124, pp. 172-183, DOI: 10.1016/j.soildyn.2019.05.001

Inspection of three sophisticated constitutive models based on monotonic and cyclic tests on fine sand: Hypoplasticity vs. Sanisand vs. ISA

T. Wichtmann[i] ; W. Fuentes[ii]; Th. Triantafyllidis[iii]

Abstract: The prediction quality of three of the most sophisticated constitutive models for sands has been examined based on a comparison of results from element test simulations and laboratory tests. Hypoplasticity with intergranular strain, the Sanisand elastoplastic model in the version of 2004 and the recently proposed ISA (intergranular strain anisotropy) model have been inspected. The laboratory tests performed on Karlsruhe fine sand used in the present study are freely available on the homepage of the first author. The model predictions have been inspected for drained and undrained monotonic triaxial tests with various densities and pressures and for monotonic tests with a few number of un- and reloading cycles. The main focus, however, lies on undrained cyclic triaxial tests with either stress or strain control and with different densities, initial stresses and stress/strain amplitudes. The strengths and weaknesses of the different constitutive models for various test conditions are worked out.

Keywords: constitutive models, calibration, element test simulations, comparison with laboratory data, monotonic and cyclic tests

1 Introduction

Numerical simulations of geotechnical structures under earthquake loading, which may eventually be affected by soil liquefaction, require the use of sophisticated constitutive models for the soil. For these analyses, the selected constitutive model is expected to reproduce the mechanical behavior of the soil at different stress/strain amplitudes, especially under undrained cyclic loading, whereby cyclic mobility effects and the accumulation of pore water pressure should be adequately described. Several advanced constitutive models for non-cohesive soils have been developed during the last two decades, e.g. the hypoplastic model with intergranular strain [19, 21], the Sanisand elasto-plastic model [2, 3], or most recently the ISA (intergranular strain anisotropy) model [6]. Likewise, a huge number of high-quality laboratory tests with various boundary conditions and control has been performed by the authors at the Institute of Soil Mechanics and Rock Mechanics (IBF) at Karlsruhe Institute of Technology (KIT) during the last decade. The experimental database has been published in [24, 25] and made freely available on the homepage of the first author [23]. The data enable the calibration, inspection and further development of constitutive models for granular materials, considering as many different boundary conditions and types of control as possible. Such close examination of the constitutive equations based on element tests creates confidence for an application of the model to different real problems.

The present paper documents a numerical study in which the data from [23–25] have been used to inspect three of the most sophisticated models mentioned above: Hypoplasticity with intergranular strain, the Sanisand elastoplastic model in the version of 2004 and the first version of ISA model (version 2014). Alternative or improved versions of Sanisand [20], Hypoplasticity [17, 18] and ISA [7–9] have been proposed in the meantime, but this paper restricts to the original and most popular versions of the models, already incorporating the most important features of those types of models. The results of element test simulations with the three models are confronted with the experimental data. The element test simulations have been performed using the program *Incremental Driver* of Niemunis [15] in combination with Abaqus implementations of the constitutive models (the so-called UMAT's) written by A. Niemunis (Hypoplasticity with intergranular strain) or W. Fuentes (ISA, Sanisand). First, the calibration of the three models is briefly explained in the next section. All experimental and theoretical research reported herein has been done during the collaborate work of all authors at the IBF at KIT.

2 Parameter calibration

The parameters of Hypoplasticity with intergranular strain for Karlsruhe fine sand are summarized in Table 1. The critical friction angle φ_c has been determined from the inclination of a loosely pluviated cone of sand. Following the parameter determination guide proposed in [10], the characteristic void ratios at $p = 0$ are estimated from the relations $e_{i0} = 1.15e_{\max}$, $e_{c0} = e_{\max}$ and $e_{d0} = e_{\min}$, where $e_{\max}$ and $e_{\min}$ are the maximum and minimum void ratios determined from standardized laboratory tests [**?**]. Parameters h_s and n were carefully calibrated to reproduce the reduction of the void ratio e with increasing mean (effective) pressure p under oedometric compression conditions on loose samples. The e-p behavior of dense samples in oedometric compression tests was then reproduced by calibrating the parameter β. The parameter α has been adjusted to reproduce the peak stress measured in drained monotonic

[i] Professor for Geotechnical Engineering, Bauhaus-Universität Weimar, Germany (corresponding author). Email: torsten.wichtmann@uni-weimar.de

[ii] Universidad del Norte, Colombia

[iii] Professor and Director of the Institute of Soil Mechanics and Rock Mechanics, Karlsruhe Institute of Technology, Germany

triaxial tests with dense samples. Parameters for the intergranular strain extension, namely R, m_R, m_T, β_R, χ, have been calibrated to reproduce the mechanical behavior of the sand in an undrained cyclic triaxial test, named TCUI7 in the database [23], with constant deviator stress amplitude $q^{\mathrm{ampl}} = 60$ kPa, initial mean effective stress $p_0 = 200$ kPa and relative density $D_r = (e_{\max} - e)/(e_{\max} - e_{\min}) \cdot 100 = 67$ % (medium dense sample). The parameters were chosen in order to achieve the best possible reproduction of the measured curves of strain amplitude $\varepsilon_1^{\mathrm{ampl}}(N)$ and pore water pressure accumulation $u^{\mathrm{acc}}(N)$. A respective comparison is provided in Section 4. Users interested in more details for the calibration of intergranular strain parameters are referred to [14, 22].

Table 2 contains the parameters of the ISA model. For this work, the same parameters reported by [6] for the same sand are used, except for the intergranular strain parameters m_R, β, χ_h and c_z which were recalibrated herein to reproduce the mechanical behavior of the undrained cyclic test TCUI7. A detailed guide for the parameter determination of the ISA model can be found in [6]. A brief description is given in the following lines: The parameters e_{i0}, λ_i, n_{pi} and n_e control the e-p behavior under oedometric compression of either loose or dense sand samples, and therefore, their calibration follows from oedometric curves. Poisson's ratio ν has been calibrated from the initial inclination of the $q(\varepsilon_1)$ curves in drained monotonic triaxial tests. The parameters e_{c0}, λ_c, n_{pc} describing the critical state line in the e-p plane have been determined from a fitting to the experimental data from numerous undrained monotonic triaxial tests performed on the fine sand (Figure 1). M_c and M_e with their ratio $c = M_e/M_c$ describe the critical state lines in the p-q plane for triaxial compression or extension, respectively. These parameters can be obtained from the inclination of the final phase of the effective stress paths under undrained monotonic triaxial tests. In the present case, M_c and M_e have been determined by calculation using the Mohr-Coulomb relations $M_c = 6 \sin\varphi_c/(3 - \sin\varphi_c)$ and $M_e = -6 \sin\varphi_c/(3 + \sin\varphi_c)$ with the critical friction angle $\varphi_c = 33.1°$. The parameters n_d and f_{b0} controlling the intensity of dilatancy and the peak of the stress-strain curves, respectively, were determined based on the curves of volumetric strain $\varepsilon_v(\varepsilon_1)$ and deviatoric stress $q(\varepsilon_1)$ measured in a drained monotonic triaxial test with initially dense state.

It is worth to mention, that the recent version of ISA model [9] uses the same parameters of the hypoplastic model for sands for monotonic loading (e_{i0},e_{c0}, e_{d0}, h_s, n, α and β), which makes its calibration simpler for users of Hypoplasticity.

The parameters of the Sanisand elastoplastic model for Karlsruhe fine sand are summarized in Table 3. The parameters were calibrated according to the following procedure: Parameters e_0, λ and ξ describe the critical state in the e-p plane derived again from the data in Figure 1. M_c and M_e are the same parameters as used in the ISA model and thus calibrated in the same way. The parameter $m = 0.05$ describing the shape of the cone-type yield surface has been overtaken from [2] to enable a proper small-strain response. The shear modulus factor G_0 was chosen such that a realistic prediction for the initial stiffness in drained monotonic triaxial tests was obtained. A very low (and thus rather unrealistic) value of Poisson's ratio $\nu = 0.05$ is necessary

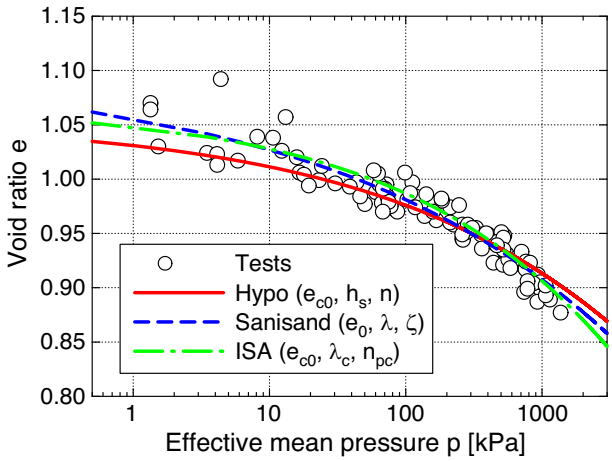

Fig. 1: *Critical state in the e-p diagram from numerous undrained monotonic triaxial tests on Karlsruhe fine sand with a variation of initial density and mean effective stress, and its approximation by the equations incorporated in the three inspected constitutive models*

in this model to achieve an oedometric stiffness that comes close to the experimental data. The parameters h_0 and c_h of the plastic modulus have been varied until the best possible agreement of the simulated and the measured stress-strain relationships $q(\varepsilon_1)$ in the drained monotonic triaxial tests was reached. The parameter n_b was adopted to reproduce the peak deviatoric stresses measured in these tests, while the constants n_d and A_0 controlling the dilatancy were chosen to reproduce the volumetric response $\varepsilon_v(\varepsilon_1)$ best possible. The parameters $z_{\max}$ and c_z were selected to reproduce the cyclic mobility effect of the test TCUI7. The parameters G_0 and h_0 obtained from tests with monotonic loading were slightly adjusted based on the cyclic test in order to achieve a better reproduction of stiffness and pore water pressure accumulation.

3 Inspection based on data from monotonic tests

Figure 2 presents simulations of oedometric compression tests on loose and dense samples with a single un- and reloading cycle. The simulations have been started at $\sigma_1 = 1$ kPa. In case of the hypoplastic and ISA models, the intergranular strain has been assumed to be initially fully mobilized in the vertical direction. Since the parameters h_s, n and β of the hypoplastic model and λ_i, n_{pi} and n_e of the ISA model have been calibrated to reproduce the first loading curves of these oedometric tests, the good prediction of these models at this phase of the test is evident. The oedometric stiffness upon unloading is also well reproduced by both models. However, both models show a weak performance during the final stage of reloading for the loose case (upper row in Figure 2). For the dense case (lower row in Figure 2), Hypoplasticity overestimates the stiffness at the reloading phase, leading to an overshooting effect. The shear stiffness parameter G_0 of the Sanisand model has been calibrated from cyclic triaxial tests. Having parameter G_0 fixed, the oedometric stiffness can be solely influenced by Poisson's ratio ν. The diagrams in Figure 2e,f reveal, however, that even a very low value of $\nu = 0.05$ still leads to an overestimation of stiffness, in particular in case of loose samples. Probably, a better agreement of experi-

φ_c [°]	e_{i0} [-]	e_{c0} [-]	e_{d0} [-]	h_s [MPa]	n [-]	α [-]	β [-]	R [-]	m_R [-]	m_T [-]	β_R [-]	χ [-]
33.1	1.212	1.054	0.677	4000	0.27	0.14	2.5	10^{-4}	2.2	1.1	0.1	5.5
CP[i]	ST[ii]	ST	ST	OED[iii]	OED	DMT[iv]	OED	UCT[vi]	UCT	UCT	UCT	UCT

[i]CP Cone pluviation test
[ii]ST Standard test on minimum and maximum density
[iii]OED Oedometric test
[iv]DMT Drained monotonic triaxial test
[v]UMT Undrained monotonic triaxial test
[vi]UCT Undrained cyclic triaxial test
[vii]CSL Critical state line in *e-p* space

Table 1: Material parameters of Hypoplasticity with intergranular strain for Karlsruhe fine sand used for the simulations. The last row presents the tests used for the calibration of the corresponding parameter.

e_{i0} [-]	λ_i [-]	n_{pi} [-]	n_e [-]	ν [-]	e_{c0} [-]	λ_c [-]	n_{pc} [-]	M_c [-]	c [-]	n_d [-]	f_{b0} [-]	R [-]	m_R [-]	β [-]	χ_h [-]	c_z [-]	r_F [-]
1.21	0.0045	0.8	3.2	0.35	1.067	0.00573	0.68	1.34	0.7	0.5	1.8	10^{-4}	1.7	0.1	11	50000	1.6
OED	OED	OED	OED	UMT[v]	CSL[vii]	CSL	CSL	UMT	UMT	DMT	DMT	UCT	UCT	UCT	UCT	UCT	DMT

Table 2: Material parameters of ISA (2014) model for Karlsruhe fine sand used for the simulations. The last row presents the tests used for the calibration of the corresponding parameter (see Table 1 for acronyms).

mental and numerical oedometric curves can be achieved by employing the version 2008 of the Sanisand model [20], which incorporates a wedge-type yield surface with a cap.

Simulations of three drained monotonic triaxial tests with different densities and an initial mean effective stress $p_0 = 100$ kPa are shown in Figure 3. For this and subsequent simulations with isotropic initial stresses, a fully isotropic mobilization of the initial state of the intergranular strain has been assumed, i.e. $h_{ii} = -R/\sqrt{3}$. This is justified with the preceding isotropic increase of effective stress towards p_0. From these simulations, one may note that the peak strength is fairly well reproduced by the hypoplastic and ISA models. This could be expected since parameters α (Hypoplasticity), and f_{b0} (ISA) have been carefully calibrated to reproduce the peak strength of these tests. The Sanisand model shows a disagreement of the $q(\varepsilon_1)$-curves before reaching the peak strength, because the parameters G_0 and h_0 have been optimized to reproduce a cyclic loading test and not monotonic loading. The volumetric strain behavior $\varepsilon_v(\varepsilon_1)$ in Figure 3 (lower row) is well reproduced by Sanisand and ISA models considering that both models offer the possibility to control these curves independently of the peak strength behavior: parameters n_d and r_F of the ISA model and n_d and A_0 of the Sanisand model can be calibrated to reproduce the $\varepsilon_v(\varepsilon_1)$-curves once the parameters for the critical state line at the *e-p* space are fixed. The hypoplastic model does not show an agreement on the $\varepsilon_v(\varepsilon_1)$ curves, because its parameter α controlling these curves was previously calibrated to reproduce the peak stress of the test. It is obvious that Hypoplasticity has a clear disadvantage against the other two models considering that it does not offer any independent parameter to control the $\varepsilon_v(\varepsilon_1)$ behavior under drained triaxial conditions.

The results from simulations of four drained triaxial tests with different initial pressures $p_0 = \{50, 100, 200, 400\}$ kPa performed on samples with medium density ($57\% < D_{r0} < 68\%$) are provided in Figure 4. The pressure-dependence of shear strength is well described by the three models. Once more, the $\varepsilon_v(\varepsilon_1)$ behavior is well assessed by the Sanisand and ISA models, while a disagreement is observed in case of the hypoplastic model.

Figure 5 presents simulations of undrained monotonic triaxial tests starting at a mean effective stress of $p_0 =$ 200 kPa, and having different initial densities. Compressional and extensional triaxial shearing are included. The simulations show a general agreement with the measured $q(\varepsilon_1)$-curves (see Figure 5, lower row) while a lack of accuracy on the effective stress paths in the *q-p* space is observed. Probably, the best simulations are provided by the hypoplastic model because it incorporates a parameter m_T controlling the transverse stiffness, which strongly influences the behavior during an undrained shearing in the *q-p* space after the isotropic consolidation phase. The ISA and Sanisand models do not incorporate parameters controlling the transverse stiffness, and therefore their simulations are deficient at this stage (a recent development of the ISA model has now tackled this issue [9]). All models show a poor reproduction of the development of pore water pressure, considering that most parameters controlling the *q-p* behavior were calibrated to simulate the cyclic (and not monotonic) behavior under undrained conditions. Note also, that the Sanisand model predicts higher stress ratios q/p than measured in the experiment. This last observation is disappointing, considering that the parameter n_b was carefully calibrated with the maximum stress ratios observed in the drained triaxial tests to reproduce the material's bounding surface. This drawback corroborates some ideas of other authors pointing to the fact that the bounding surface of the soil cannot be fully described with the mean effective stress p and void ratio e for all stress-strain paths [18], as assumed by the Sanisand model.

Figure 6 presents simulations of a drained monotonic test interrupted by four unloading (to $q = 0$) with subsequent reloading phases. The initial effective mean stress was $p_0 = 100$ kPa and the sample was medium dense (D_{r0} = 62 %). The axial strain increment between two adjacent unloadings was chosen as $\Delta\varepsilon_1 = 6$ %. The results show that the employed constitutive models deliver a lower

e_0 [-]	λ [-]	ξ [-]	M_c [-]	M_e [-]	m [-]	G_0 [-]	ν [-]	h_0 [-]	c_h [-]	n_b [-]	A_0 [-]	n_d [-]	$z_{\max}$ [-]	c_z [-]
1.103	0.122	0.205	1.34	0.938	0.05	150	0.05	10.5	0.75	1.2	0.9	2.0	20.0	10000
CSL	CSL	CSL	UMT	UMT	-	DMT, UCT	OED	DMT, UCT	DMT	DMT	DMT	DMT	UCT	UCT

Table 3: Material parameters of Sanisand (2004) model for Karlsruhe fine sand used for the simulations. The last row presents the tests used for the calibration of the corresponding parameter (see Table 1 for acronyms).

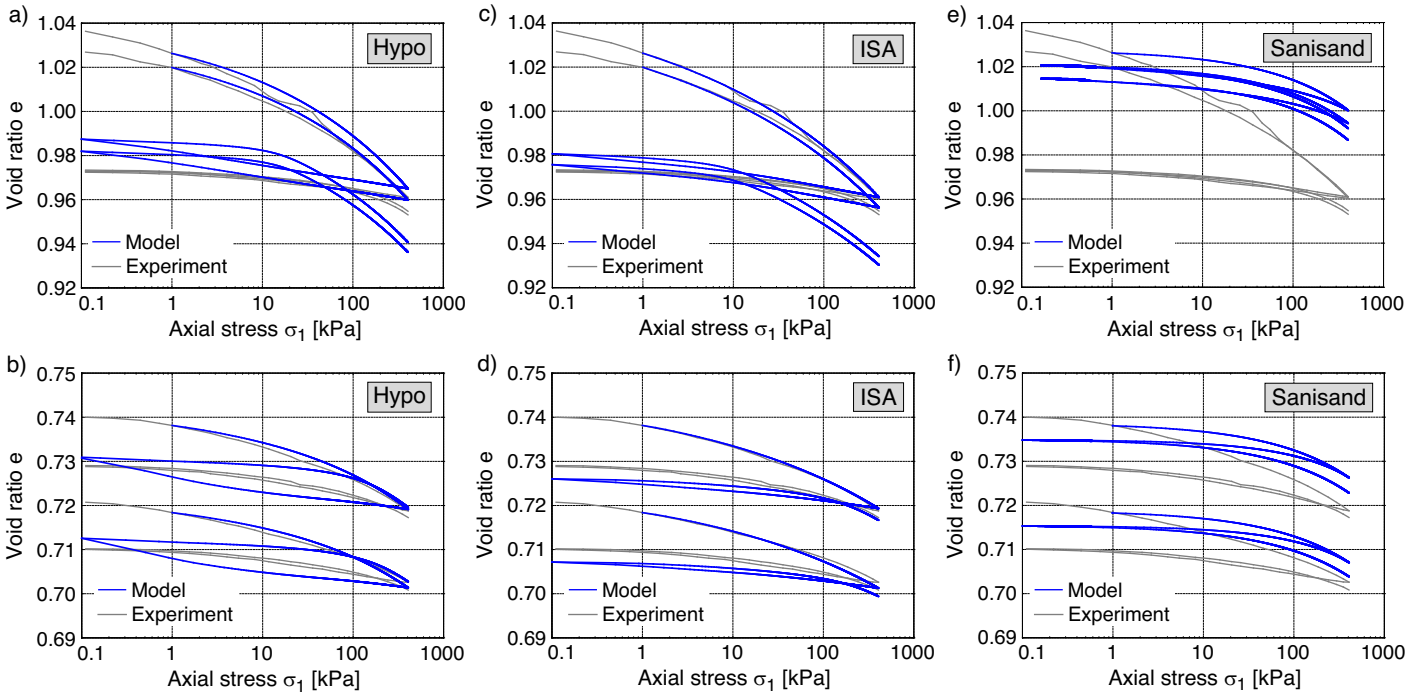

Fig. 2: *Simulations of oedometric compression tests on loose (D_{r0} = 4 % and 7 %, upper row) or dense samples (D_{r0} = 83 % and 88 %, lower row) with a single un- and reloading cycle: a,b) Hypoplasticity with intergranular strain, c,d) ISA, e,f) Sanisand*

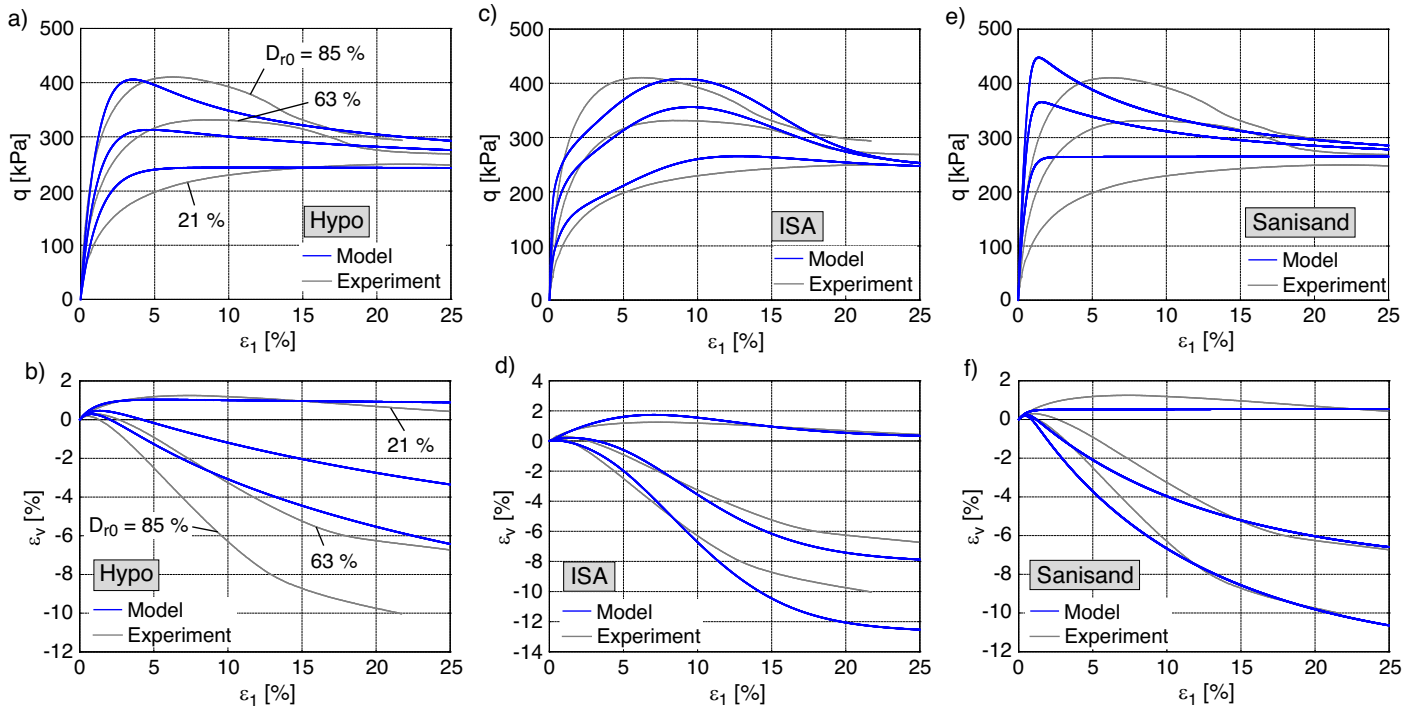

Fig. 3: *Simulations of drained monotonic triaxial tests with different initial densities (D_{r0} = 21 %, 63 %, 85 %) and an initial mean effective stress p_0 = 100 kPa: a,b) Hypoplasticity with intergranular strain, c,d) ISA, e,f) Sanisand*

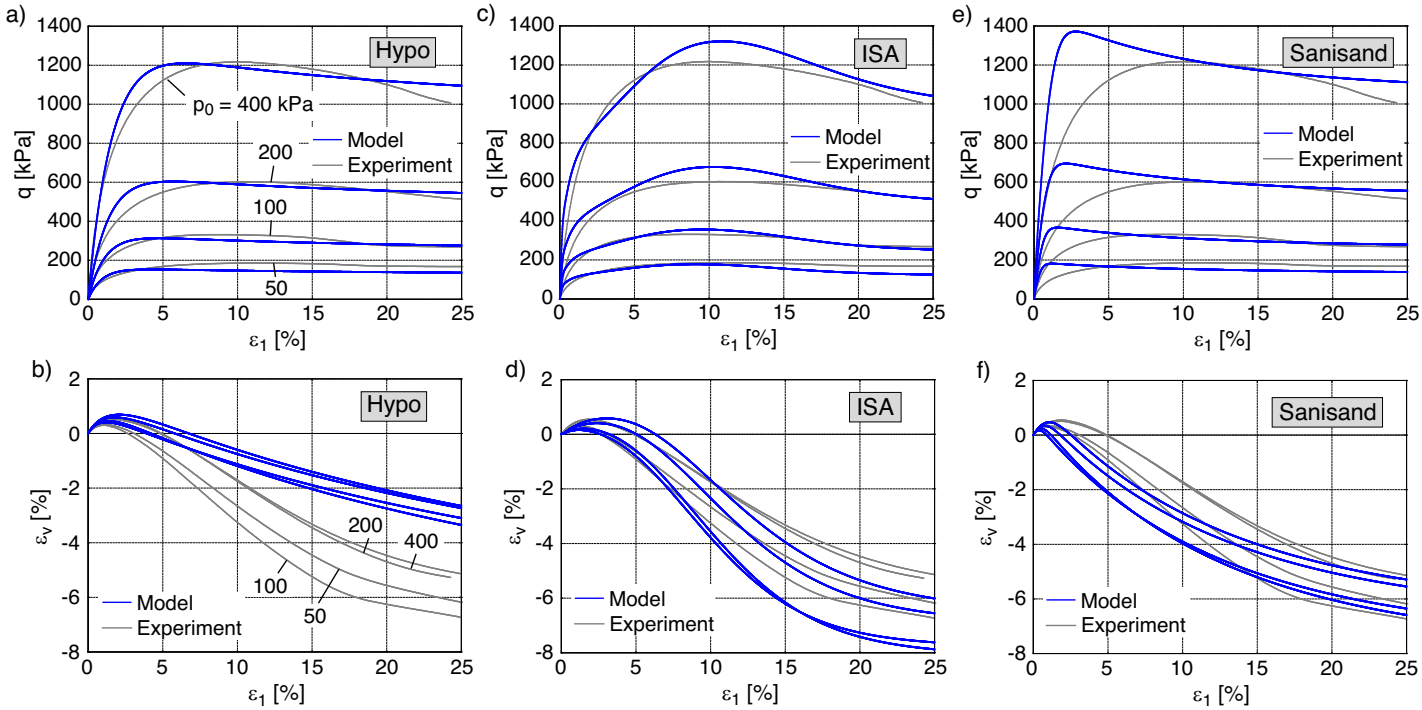

Fig. 4: *Simulations of drained monotonic triaxial tests on medium dense samples (57 % ≤ D_{r0} ≤ 68 %) with different initial pressures p_0 = 50, 100, 200 or 400 kPa: a,b) Hypoplasticity with intergranular strain, c,d) ISA, e,f) Sanisand*

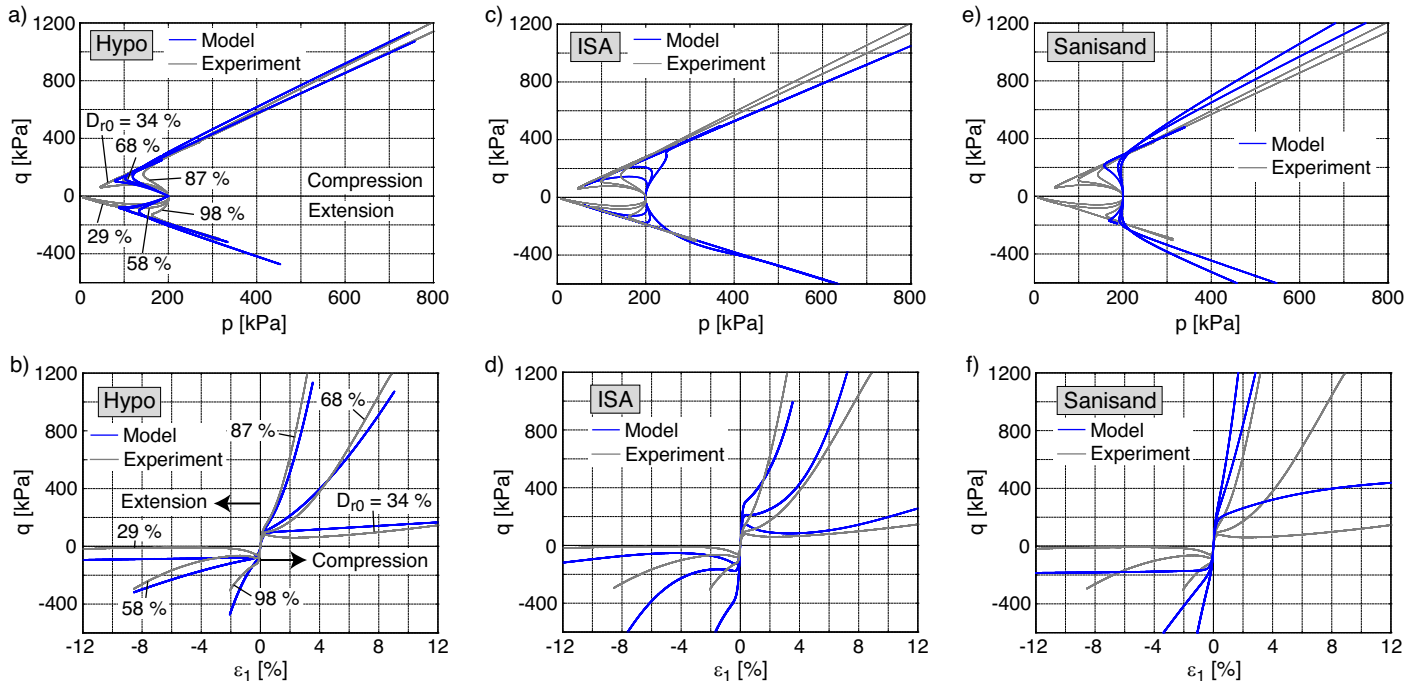

Fig. 5: Simulations of undrained monotonic triaxial tests with different initial densities (D_{r0} = 34, 68, 87 % in triaxial compression, D_{r0} = 29, 58, 98 % in triaxial extension): a,b) Hypoplasticity with intergranular strain, c,d) ISA, e,f) Sanisand

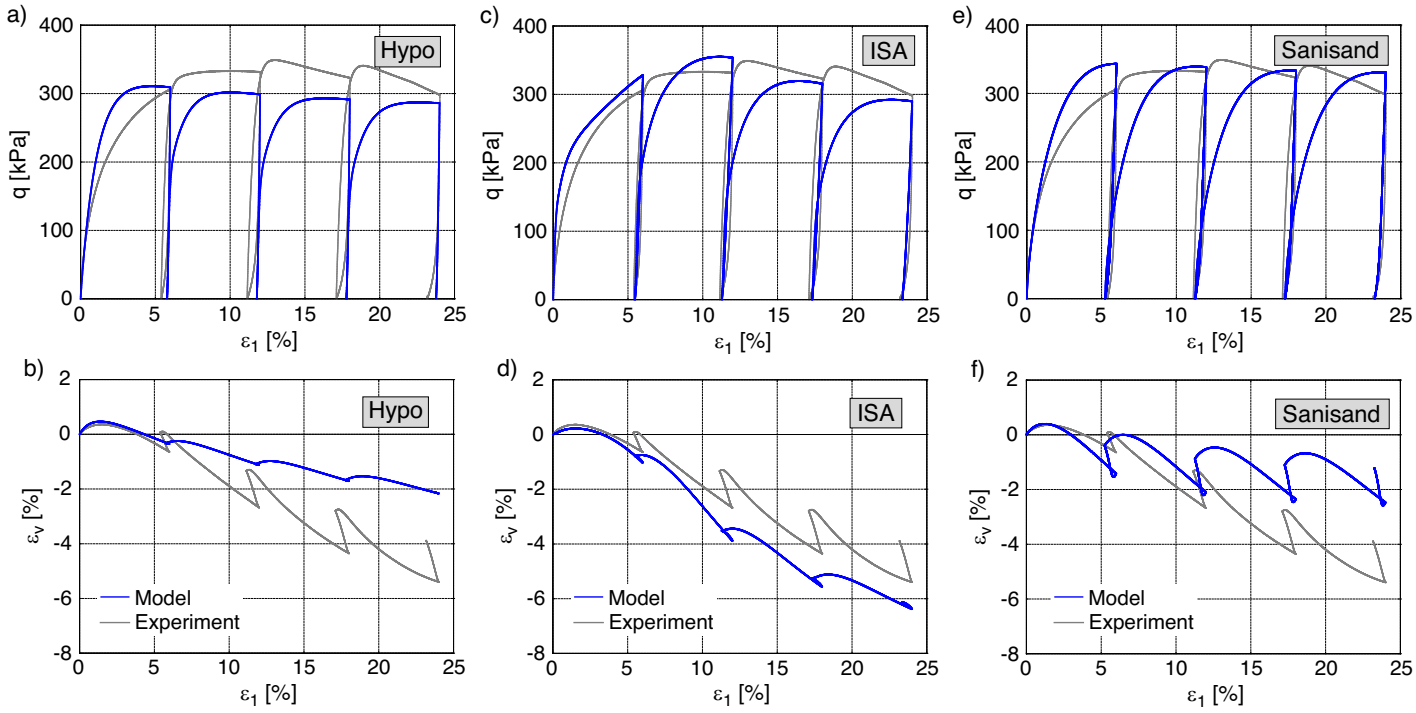

Fig. 6: *Simulations of a drained monotonic triaxial test interrupted by an unloading to $q = 0$ after each strain increment $\Delta\varepsilon_1 = 6\%$ ($p_0 = 100$ kPa, $D_{r0} = 62$ %): a,b) Hypoplasticity with intergranular strain, c,d) ISA, e,f) Sanisand*

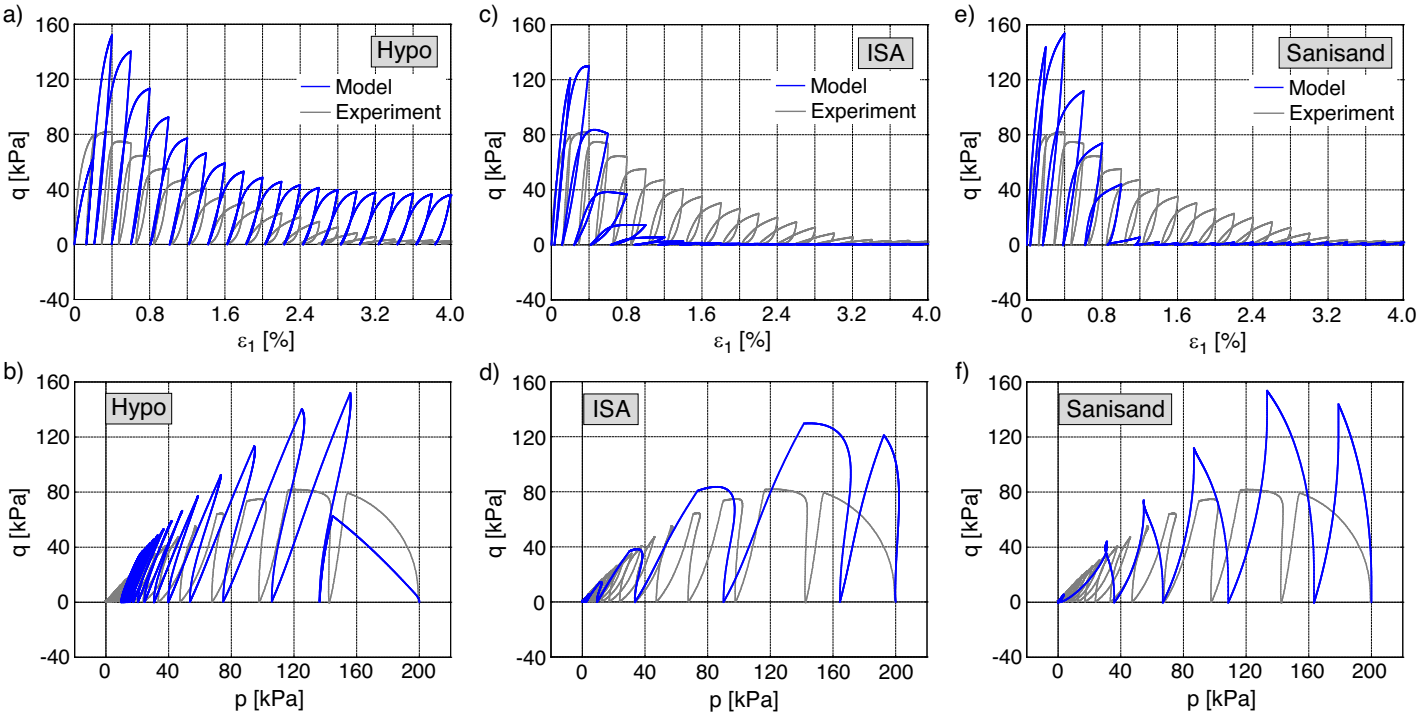

Fig. 7: *Simulations of an undrained monotonic triaxial test interrupted by an unloading to $q = 0$ after each strain increment $\Delta\varepsilon_1 = 0.2\%$ ($p_0 = 200$ kPa, $D_{r0} = 23$ %): a,b) Hypoplasticity with intergranular strain, c,d) ISA, e,f) Sanisand*

stiffness during the final phase of reloading as observed in the experiments. This issue is explained with the fact, that although the three models incorporate some mechanisms to capture the small-strain effects, the latter are limited to some strain amplitudes which depend on the selected parameters. In contrast, experiments involving unloading-reloading cycles of medium or large strain amplitudes have shown an enlargement of the strain amplitude at which the small strain effects should act. This enlargement is for example evident at the reloading stages on the oedometric tests, especially on loose samples, see Figure 2 (first row). Some new Sanisand-type models already include "initialization tensors" intending to improve this behavior [1] under undrained conditions.

An inspection of the model performance based on a similar test under undrained conditions is shown in Figure 7. A loose sample (D_{r0} = 23 %) was tested with an initial mean effective stress of p_0 = 200 kPa. An unloading to q = 0 was performed every $\Delta\varepsilon_1$ = 0.2 %. The hypoplastic simulation shows a clear example of "overshooting" of the effective stress path during the first reloading. The overshooting effect is actually a serious limitation in this and other models. As a matter of fact, one of the authors of the model admits to be aware about this drawback, which is shown by this and other models, such as the Hardening Soil (HS) Small Strain model included in the software Plaxis [16]. Though this disagreement, the accumulation of the pore water pressure upon the cycles is realistically simulated by the hypoplastic model. The ISA and Sanisand models show a higher accumulation rate of the pore water pressure. Such larger accumulation rate is certainly accompanied by an unrealistically rapid decrease of the maximum deviatoric stresses reached during the individual cycles (see q-ε_1 diagrams in Figure 7c,e).

4 Inspection based on data from undrained cyclic tests

Selected undrained cyclic triaxial tests performed on KFS have been simulated with the three constitutive models. Simulations of the undrained cyclic test TCUI7 already mentioned in Section 2 are shown in Figure 8. One may note that the effective stress path is fairly well reproduced by the Sanisand and ISA models, showing an accurate reproduction of the butterfly-like shape during the cyclic mobility phase (Figure 8c,e). Hypoplasticity delivers a too contractive response during the first cycle and an unrealistic lens-shaped effective stress path during the final stage of the test. Contrary to the experiment, this model does not reach a zero effective mean stress ($p = 0$) at the end of the test. Evidently, this drawback is explained with the fact, that while the formulations of the ISA and Sanisand models have been extended by an additional tensorial state variable to reproduce the cyclic mobility paths, Hypoplasticity uses the same equation without any modification. Looking at the stress-strain relationships (Figure 8b,d,f), it is evident that the hypoplastic and Sanisand models show a strong bias in strain accumulation during the cyclic mobility phase. The latter drawback can be attributed to the following reasons: first of all, these models incorporate different slopes of the critical state lines for compression and extension in the q-p space, denoted by M_c and M_e respectively. Hence, for these undrained cyclic paths, a larger strain accumulation is always obtained at the extension side ($q < 0$) than on the compression side ($q > 0$). The ISA model does not show this bias in strain accumulation because although the model considers the slopes M_c and M_e as well, its dilatancy, and therefore its stress hardening under undrained shearing, is strongly controlled by a fabric tensor which evolves with the deviatoric strain tensor. This fabric tensor forces the critical state line in the e-p space to be reached after a certain amount of deviatoric strain, similar to other formulations in the literature [4, 5, 11–13]. With this mechanism, the model is able to reproduce almost symmetrical "wings" during the cyclic mobility phase in the q-ε_1 space (Figure 8d). Despite of this achievement, one may note that the ISA model ceases to accumulate the axial strain when reaching a value of approximately $|\varepsilon_1| \approx 3$ %, in contrast to the experimental result, where the strain amplitude during the cyclic mobility phase grows with increasing number of cycles. The latter drawback is related to the fact, that the model fails to degrade the stiffness during the cyclic mobility phase.

Figures 9a and 9b compare the measured and simulated curves in test TCUI7 of the normalized accumulated pore water pressure $u^{\mathrm{acc}}(N)/p_0$ and the axial strain amplitude $\varepsilon_1^{\mathrm{ampl}}(N)$, respectively. The results show that the pore pressure accumulation rate and axial strain amplitude are well reproduced by the models. Since u^{acc} has been evaluated at $q = 0$ after the completion of a full cycle, a ratio of u^{acc}/p_0 = 1 is neither reached by Hypoplasticity nor by ISA, but almost by Sanisand (compare the effective stress paths in Figure 8a,c,e). Figure 9c presents the development of the maximum axial strain $|\varepsilon_1|$ reached under triaxial compression ($q > 0$) and extension ($q < 0$) during the last 10 cycles. Once more this diagram confirms that Hypoplasticity and the Sanisand model show a bias in strain accumulation upon the cyclic mobility phase.

Simulations of a similar test (nominated TCUI1 in the database [23]) on a loose sample (D_{r0} = 27 %) are shown in Figure 10. In contrast to the experimental evidence, the three models predict a butterfly-shaped effective stress path during the final stage of the test. The rate of pore water pressure accumulation $\dot{u}^{\mathrm{acc}}$ simulated by the hypoplastic model is closer to the test results than that of ISA and Sanisand (too large $\dot{u}^{\mathrm{acc}}$ values). The axial strain amplitude during the cyclic mobility phase simulated by the ISA model obviously increases with decreasing density (here $|\varepsilon_1| \approx 8$ %, Figure 10d).

The performance of the three models in case of dense sand (D_{r0} = 87 %, test TCUI17, Figure 11) does not differ much from that for medium dense sand (Figure 8). All three models overestimate the rates of pore water accumulation $\dot{u}^{\mathrm{acc}}$. Once more, Hypoplasticity and the Sanisand model generate a bias in the extensional strain with almost constant rate during the cyclic mobility phase, while the strains predicted by the ISA model are limited to $|\varepsilon_1| \approx$ 1.5 %.

The variation of the pore water pressure accumulation rate with density and stress amplitude is further inspected in Figure 12. Therein the amplitude-pressure ratio $CSR = q^{\mathrm{ampl}}/(2p_0)$ is plotted versus the number of cycles N required to reach the onset of large axial strain generation $|\varepsilon_1| > 1$ %. This criterion is used as a synonym for initial liquefaction since not all models reach u^{acc}/p_0 = 1 (see Figure 9a). Simulations of undrained cyclic tests with an initial mean effective stress of p_0 = 100 kPa, con-

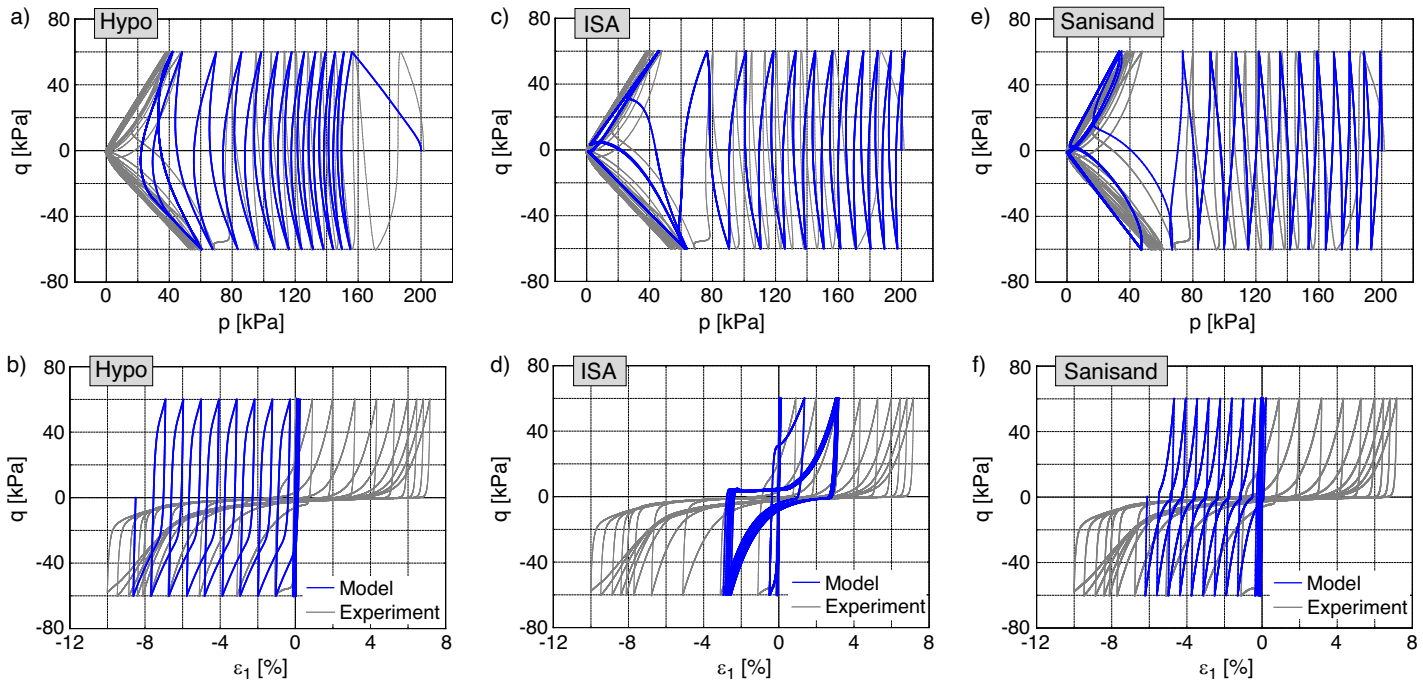

Fig. 8: Simulations of undrained cyclic triaxial test TCUI7 on a medium dense sample (D_{r0} = 67 %) with isotropic consolidation (p_0 = 200 kPa, η_0 = 0) and stress cycles (q^{ampl} = 60 kPa): a,b) Hypoplasticity with intergranular strain, c,d) ISA, e,f) Sanisand

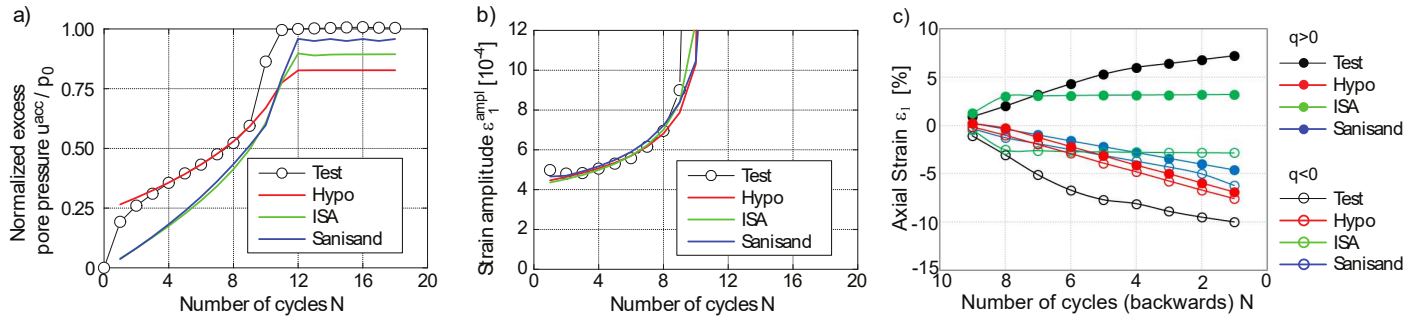

Fig. 9: *Comparison of the results of the simulations using the three different constitutive models with the experimental data of test TCUI7: a) normalized accumulated pore water pressure $u^{acc}(N)/p_0$, b) axial strain amplitude $\varepsilon_1^{ampl}(N)$, c) maximum absolute values of axial strain $|\varepsilon_1|$ in compression and extension during the last 10 cycles*

sidering three different densities (D_{r0} = 26, 63 and 81 %, corresponding to average values from laboratory test series) and different stress amplitudes have been performed. The $CSR(N)$-curves resulting from these simulations are confronted with experimental data (CSR versus number of cycles to $|\varepsilon_1| > 1$ %). Sanisand and ISA deliver quite similar $CSR(N)$-curves, being, however, much steeper than the experimental $CSR(N)$-curves. Hypoplasticity seems to capture better the CSR dependence. Nevertheless, all models show an underestimation of the influence of the density on the $CSR(N)$-curves. The experience of the authors with these models is, that some parameters controlling the accumulation rate upon cyclic loading seem to show a density-dependence, although these models are thought to simulate a wide range of void ratios.

Figure 13 shows simulations of a test (TCUA16) on a medium dense sample (D_{r0} = 56 %) with stress cycles after anisotropic consolidation. In this test the deviatoric stress amplitude q^{ampl} was larger than the initial deviatoric stress q_0, i.e. the effective stress path crosses the p axis. The stress paths in the $q-p$ space simulated by the hypoplastic model ends up with unrealistic lens-shaped loops, while the unsymmetrical butterfly-shaped path generated by ISA and Sanisand is close to the experimental observations. Larger discrepancies between the test results and the simulations can be found in the stress-strain relationships. The experiment shows a somewhat larger increase of the maximum (compressional) axial strain compared to the minimum (extensional) one. This observation is best reflected by the ISA model. However, the restriction of axial strains achievable by this model is visible also in Figure 13d. Similar to the isotropic tests, during cyclic mobility Hypoplasticity and Sanisand predict an accumulation of axial strain of almost constant rate (here in the compressional direction).

Figure 14 inspects the case of another test on medium dense sand (D_{r0} = 64 %) with anisotropic consolidation, but now $q^{\mathrm{ampl}} < q_0$ holds, such that the effective stress path lies completely in the compressional regime of the p-q plane ($q > 0$). In agreement with the experiment (TCUA2), all simulations end up in a lens-shaped effective stress path re-

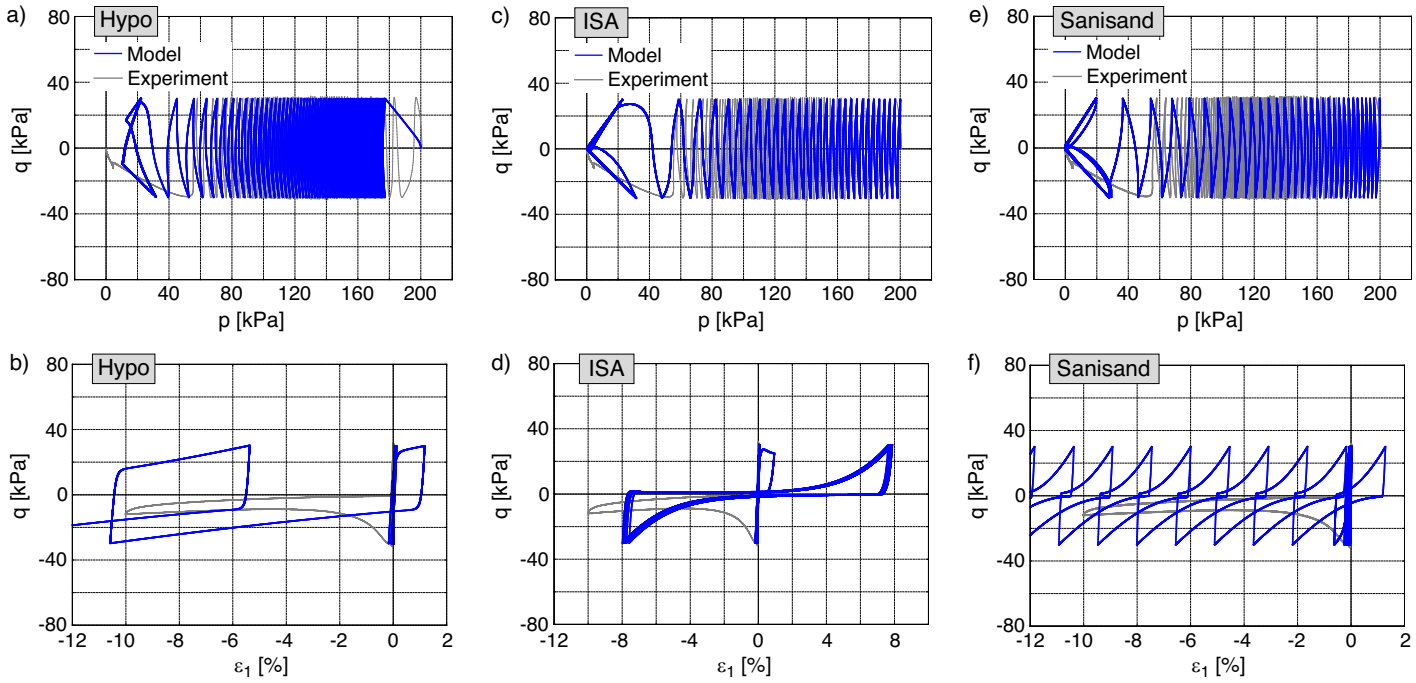

Fig. 10: Simulations of undrained cyclic triaxial test TCUI1 on a loose sample (D_{r0} = 27 %) with isotropic consolidation (p_0 = 200 kPa, η_0 = 0) and stress cycles (q^{ampl} = 30 kPa): a,b) Hypoplasticity with intergranular strain, c,d) ISA, e,f) Sanisand

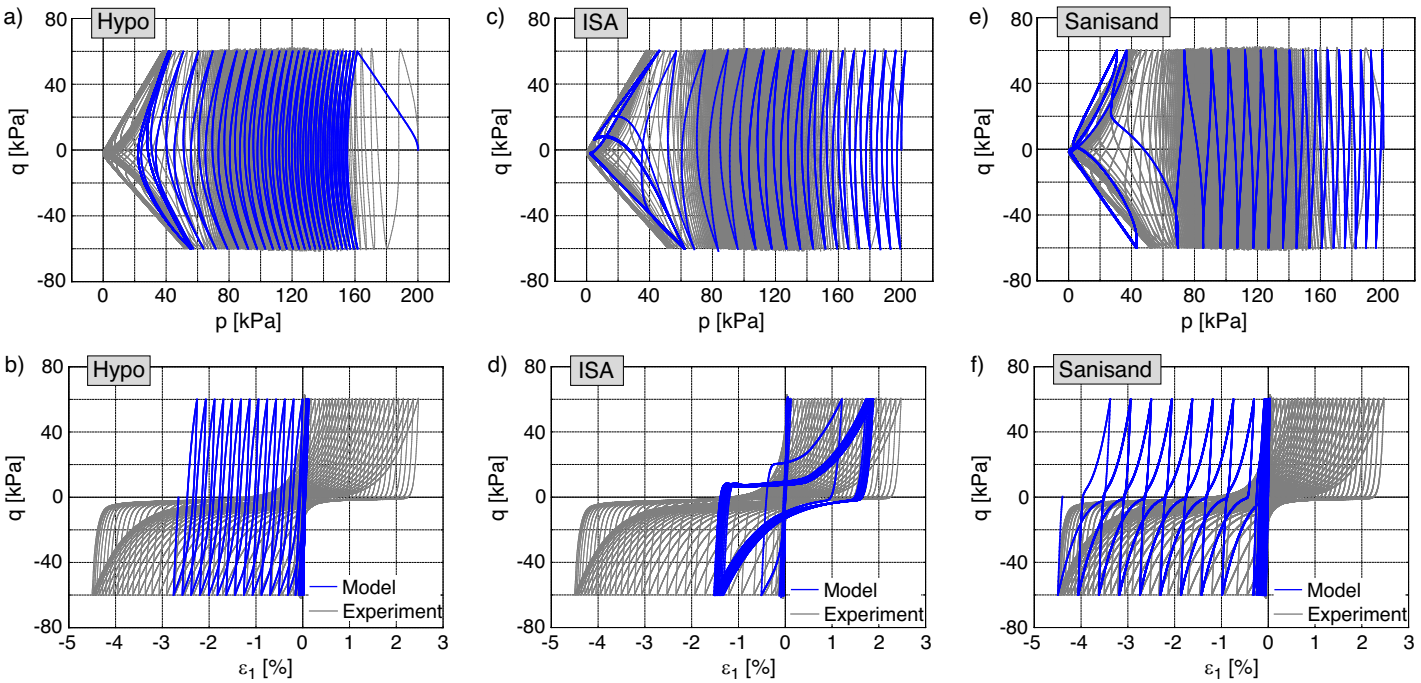

Fig. 11: Simulations of undrained cyclic triaxial test TCUI17 on a dense sample (D_{r0} = 87 %) with isotropic consolidation (p_0 = 200 kPa, η_0 = 0) and stress cycles (q^{ampl} = 60 kPa): a,b) Hypoplasticity with intergranular strain, c,d) ISA, e,f) Sanisand

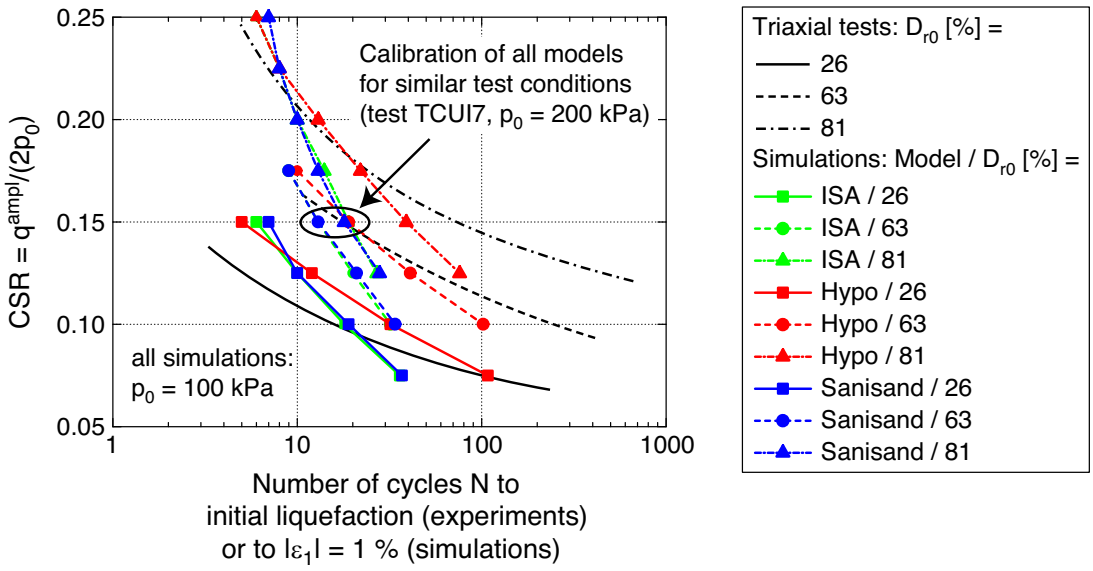

Fig. 12: *Amplitude-pressure ratio* $q^{\mathrm{ampl}}/(2p_0)$ *vs. the number of cycles* N *required to reach the onset of large axial strain generation* ($|\varepsilon_1| > 1$ %)

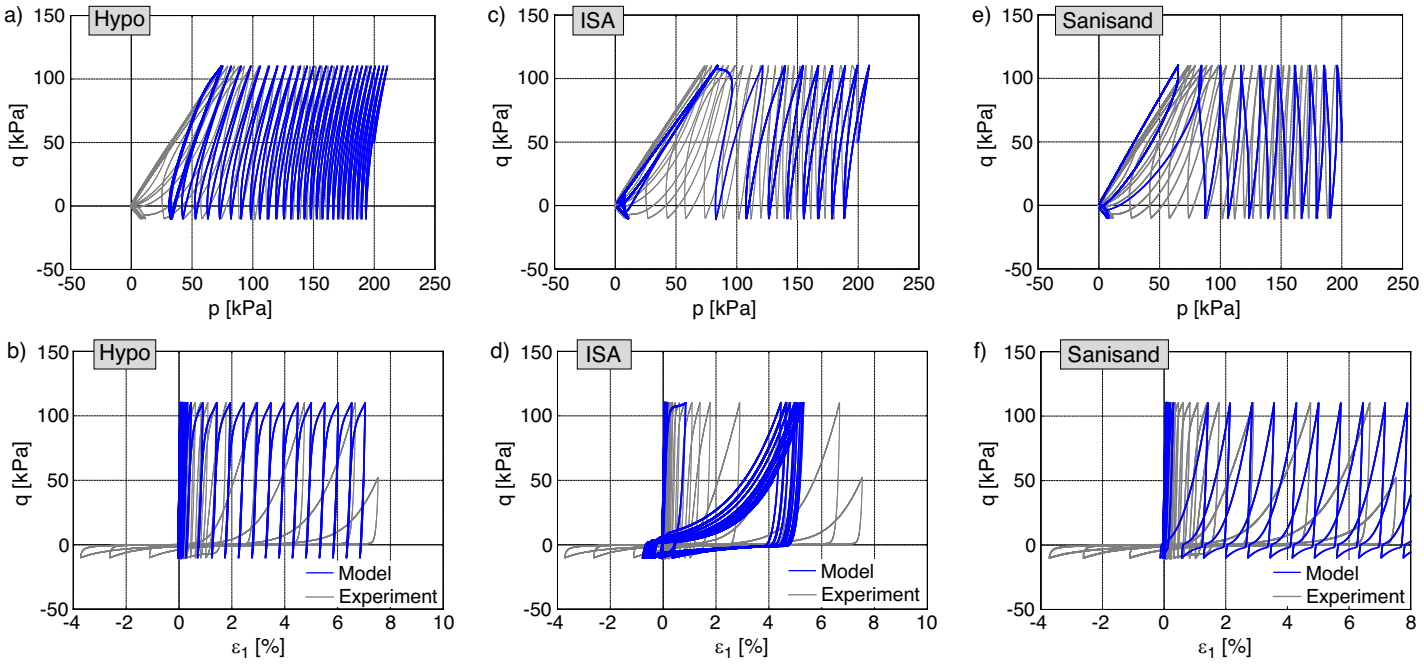

Fig. 13: Simulations of undrained cyclic triaxial test TCUA16 on a medium dense sample ($D_{r0} = 56$ %) with anisotropic consolidation ($p_0 = 200$ kPa, $q_0 = 50$ kPa, $\eta_0 = 0.25$) and stress cycles with $q^{\mathrm{ampl}} > q_0$ ($q^{\mathrm{ampl}} = 60$ kPa): a,b) Hypoplasticity with intergranular strain, c,d) ISA, e,f) Sanisand

peatedly passed through with each further cycle. However, the predicted lens is too narrow in case of Hypoplasticity and ISA, while the area encompassed by the stress path is more realistic in the results of the Sanisand simulation. The inclination of the final lens is in turn best reproduced by Hypoplasticity, while ISA and Sanisand predict an unrealistic adaption of the lens to the failure line from undrained monotonic tests. Once more, the Sanisand model fails to capture the maximum stress ratio controlled by the bounding surface of the model.

In agreement with the experiment (TCUE1), all three constitutive models reproduce the state of zero effective stress $p \approx q \approx 0$ reached after a certain number of cycles under strain cycles with relatively small amplitudes ($\varepsilon_1^{\mathrm{ampl}} = 6 \cdot 10^{-4}$, $D_{r0} = 64$ %, Figure 15). The fact that the resulting stress amplitudes are similar to those of the test indicates that the small-strain stiffness of the three models has been well adjusted, or at least, for this particular test. All three models overestimate the the pore pressure accumulation rate $\dot{u}^{acc}$, i.e. the number of cycles necessary to reach $p \approx q \approx 0$ is predicted too low. This is probably due to the fact, that the parameters controlling the accumulation rate were calibrated for a different test with different density and stress amplitude, and as mentioned before,

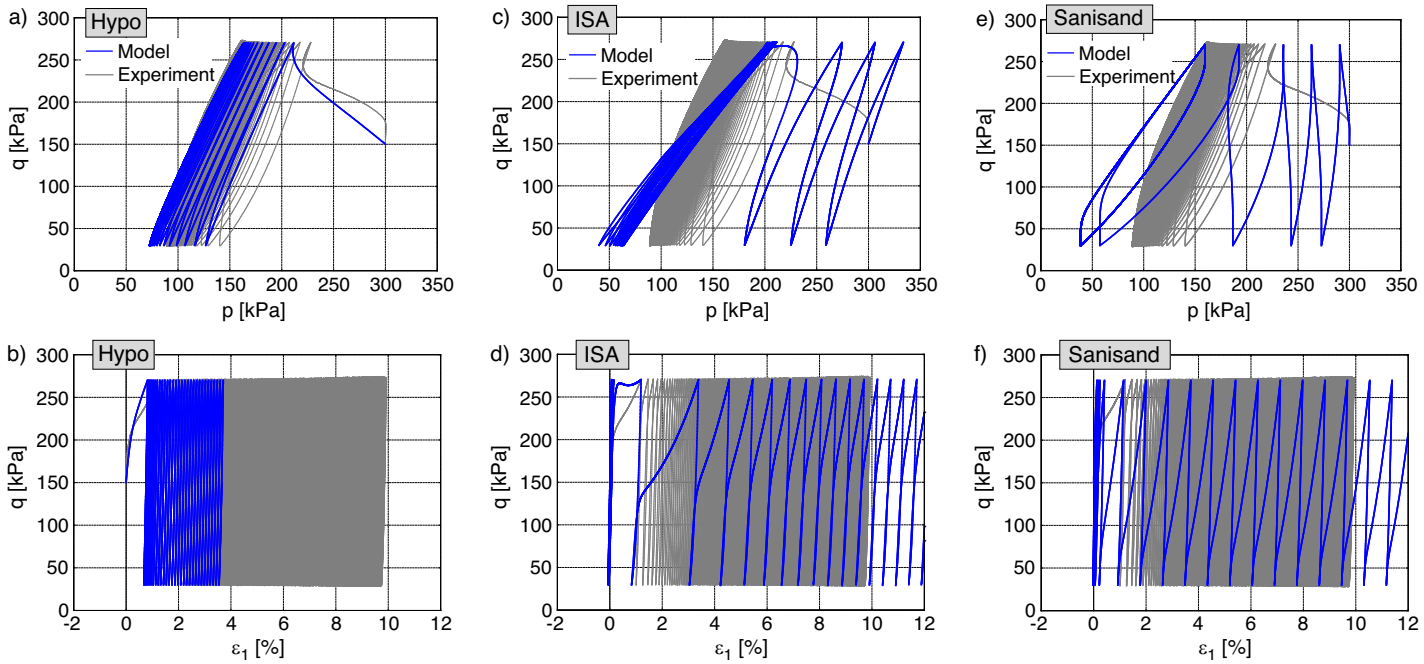

Fig. 14: Simulations of undrained cyclic triaxial test TCUA2 on a medium dense sample ($D_{r0} = 64$ %) with anisotropic consolidation ($p_0 = 300$ kPa, $q_0 = 150$ kPa, $\eta_0 = 0.5$) and stress cycles with $q^{\mathrm{ampl}} < q_0$ ($q^{\mathrm{ampl}} = 120$ kPa): a,b) Hypoplasticity with intergranular strain, c,d) ISA, e,f) Sanisand

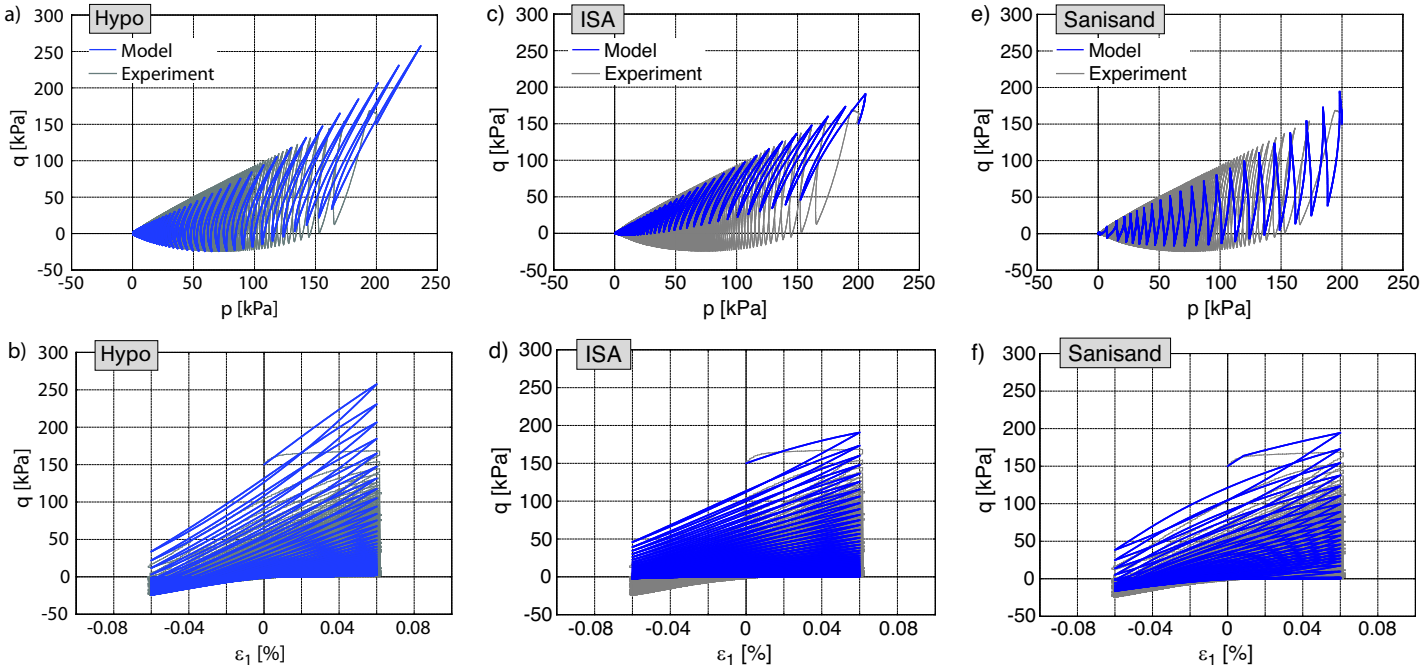

Fig. 15: Simulations of undrained cyclic triaxial test TCUE1 on a medium dense sample ($D_{r0} = 64$ %) with anisotropic consolidation ($p_0 = 200$ kPa, $q_0 = 150$ kPa, $\eta_0 = 0.75$) and strain cycles of relatively small amplitude ($\varepsilon_1^{\mathrm{ampl}} = 6 \cdot 10^{-4}$): a,b) Hypoplasticity with intergranular strain, c,d) ISA, e,f) Sanisand

these parameters have shown to be density-dependent. The stress-strain relationships provided in Figure 15b,d,f show a quite good agreement between the experiment and the simulations, especially in the case of ISA and Sanisand.

The constitutive description of the material response to large strain cycles is generally less accurate (Figure 16). In the laboratory test on dense sand (D_{r0} = 94 %, TCUE17) the effective stress path finally ends up at the origin $p = q = 0$. In contrast, the hypoplastic simulation repeatedly passes through an eight-shaped stress path, located far away from $p = 0$. Consequently, a liquefaction as observed in the experiment is not reached in the hypoplastic simulation. Of course, this is related to the fact that Hypoplasticity does not incorporate any extension accounting for cyclic mobility effects as the other models. If a dense material is simulated by this model, the dilatant effect during the cycles is stronger than the contractant effect. The large butterfly-shaped effective stress path predicted by the Sanisand model contrasts the experimental results as well, but at least $p = q = 0$ is passed temporarily. The ISA model performs better in this test, predicting a smaller butterfly.

A similar test (TCUE15) on loose sand (D_{r0} = 29 %) is investigated in Figure 17. In congruence with the test results, the effective stress path from the simulation with the ISA model comes close to $p = q = 0$. While the eight-shaped hypoplastic path stagnates at $p \approx 5$ kPa in this case, the Sanisand simulation once again ends up with an unrealistic butterfly. It is, however, somewhat smaller than in the case of dense sand.

5 Summary and conclusions

In this work, the performance of three different constitutive models for the simulation of monotonic and cyclic loading of sand has been analyzed, namely Hypoplasticity with intergranular strain, the Sanisand 2004 model and the ISA 2014 model. Their formulations consider the influence of void ratio, stress tensor, and additional internal variables to improve their prediction capabilities on cyclic loading. Hence, they are assumed to reproduce well the mechanical behavior on a wide range of densities and confining pressures. An analysis of the simulations on different tests showed that although some experimental observations are satisfactorily captured, other important features are poorly reproduced. From this analysis, the following observations related to the limitations of these models and their use on Boundary Value Problems (BVP) are highlighted:

- Simulations on oedometric tests demonstrate that models as Sanisand, which incorporates a wedge-type open yield surface, are not able to capture the oedometric behavior. This disables the model for example, to simulate correctly Boundary Value Problems (BVPs) where settlement is of interest. In some way, this limitation suggests that the yield surface shape for Sanisand-type models should be carefully reformulated in order to account for correct assessment of volumetric behavior under oedometric conditions.

- Even though these models are aimed to simulate a wide range of stress/strain amplitudes, their calibration showed that it is impossible to obtain a single set of parameters delivering accurate simulations on both monotonic and cyclic loading. To give an example, simulations of undrained monotonic shearing in Figure 5 showed in general a poor performance, considering that most parameters were calibrated to match the behavior under cyclic loading. One can show that these monotonic tests are better reproduced with other sets of parameters, at the cost of reducing the prediction capabilities on cyclic loading.

- Simulations on cyclic loading showed overshooting effects on some reloading paths, especially with the hypoplastic model. Actually, this undesired effect has been frequently observed in many advanced models. To the authors' opinion, this drawback emerges from the fact that these models lack of proper mechanisms to capture well the strain amplitude at which small-strain effects should act. It evidently cannot be captured based on an elastic locus of constant stress ratio amplitude (as by the Sanisand yield surface) or constant strain amplitude (as by the ISA and hypoplastic models). Herein, more investigation is recommended to enhance model formulations considering the mentioned observation.

- The $CSR(N)$-curves showed that all three models are still not accurate enough on the reproduction of the number of cycles required to reach the onset of large strain development, herein defined as $|\varepsilon_1| = 1$ %. Particularly, the simulations showed an underestimation of the influence of the density. This suggests that for a certain BVP, the calibration of a set of parameters should be limited to reproduce a particular small range of densities.

- The Sanisand and ISA models were able to capture fairly well the cyclic mobility effect. A bias in strain accumulation was observed on Hypoplasticity and the Sanisand model. To the authors' opinion, this drawback may not significantly affect simulations of BVPs if they are limited to a maximum strain, of approximately $\|\boldsymbol{\varepsilon}\| = 5$ %. Otherwise, excessive distortion of finite elements is also expected, or even problems related to the loss of the stress rate objectivity.

- Simulations of undrained cyclic loading with constant deviatoric stress amplitudes reached the point of zero effective stress ($q = p = 0$) only in case of loose sand. On the other hand, most models showed a ratio between the accumulated pore water pressure u^{acc} and the initial mean effective stress p_0 greater than 0.9, i.e. $u^{\mathrm{acc}}/p_0 > 0.9$ after reaching the onset of large axial strain $|\varepsilon_1| > 1$ %. This suggests that the mechanisms responsible for the cyclic mobility effects are still density-dependent, and the parameters controlling this behavior cannot be calibrated for all densities. This mechanism should be carefully revised and improved to capture better the observed behavior.

- The model parameters were adjusted to capture the maximum stress ratio observed in monotonic drained tests. However, the outcoming maximum stress ratio under undrained monotonic shearing was not well reproduced with the Sanisand model. This suggests that the bounding surface of the soil cannot be fully described only by the void ratio e and mean effective stress p as assumed by this model. Experimental corroboration of this statement can be found in [18].

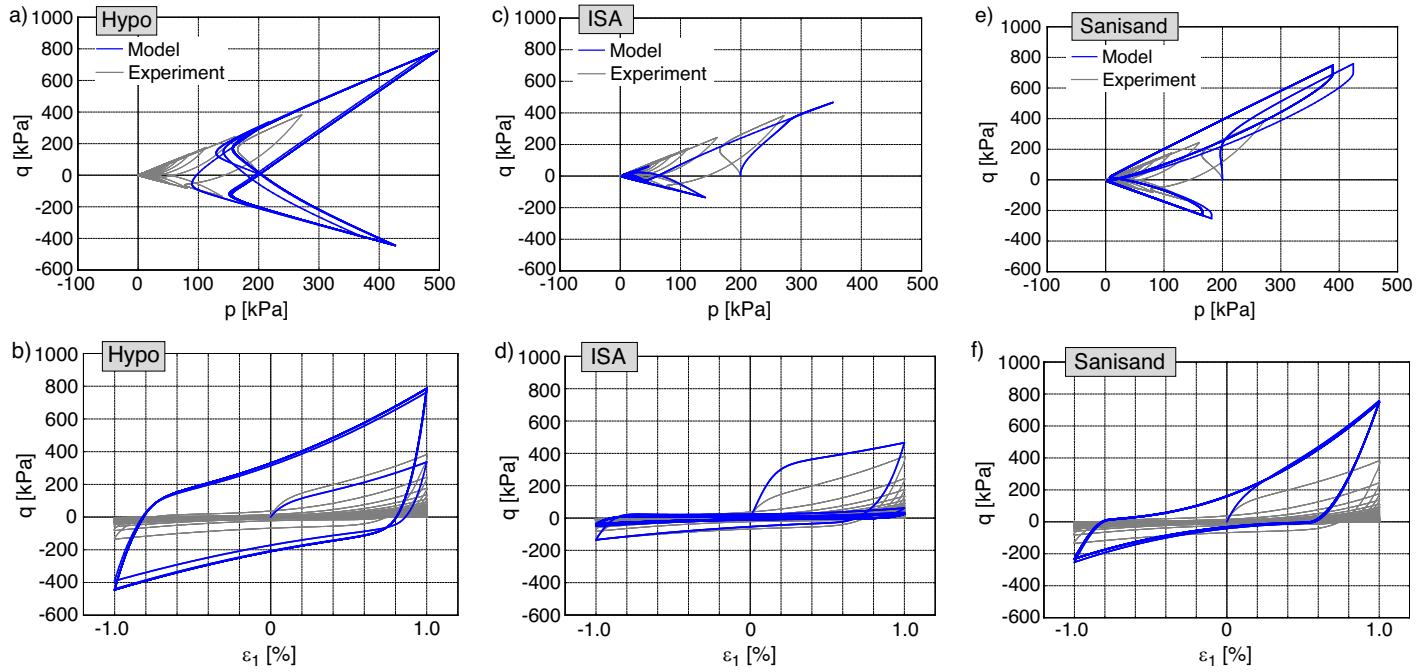

Fig. 16: Simulations of undrained cyclic triaxial test TCUE17 on a dense sample ($D_{r0} = 94$ %) with isotropic consolidation ($p_0 = 200$ kPa, $q_0 = 0$, $\eta_0 = 0$) and strain cycles of relatively large amplitude ($\varepsilon_1^{\text{ampl}} = 1 \cdot 10^{-2}$): a,b) Hypoplasticity with intergranular strain, c,d) ISA, e,f) Sanisand

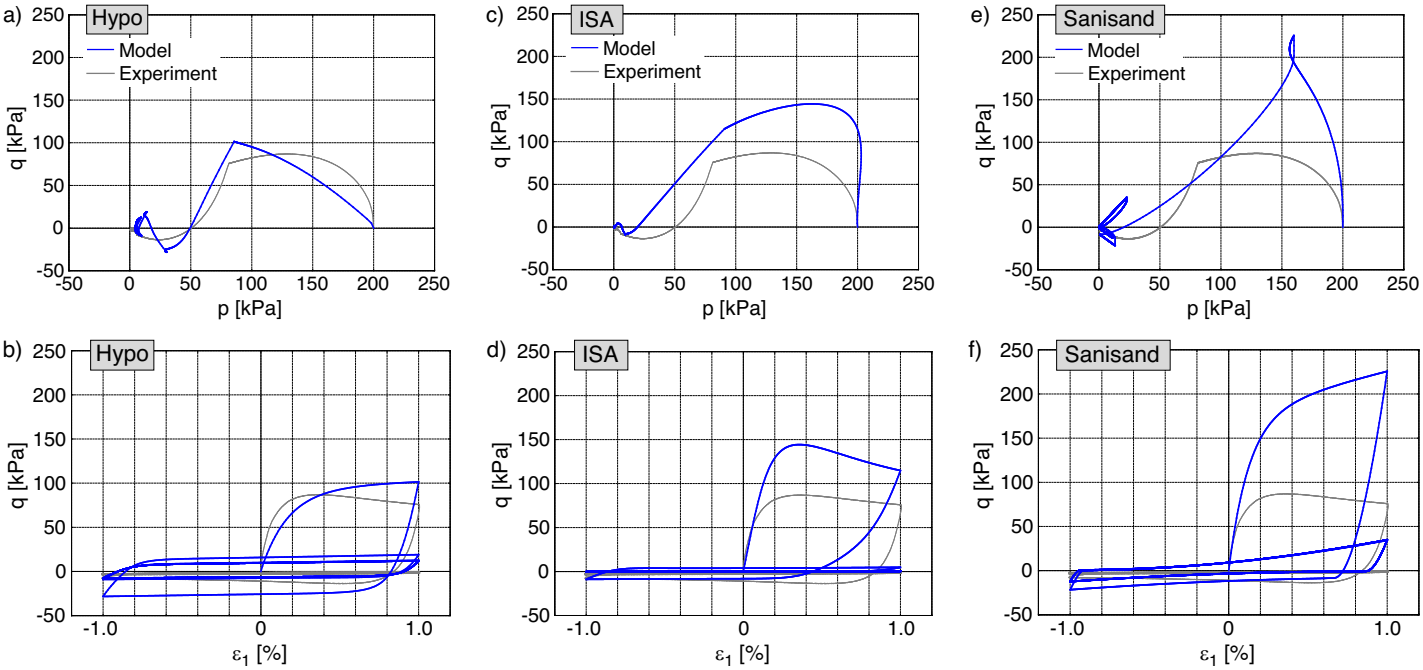

Fig. 17: Simulations of undrained cyclic triaxial test TCUE15 on a loose sample ($D_{r0} = 29$ %) with isotropic consolidation ($p_0 = 200$ kPa, $\eta_0 = 0$) and strain cycles of relatively large amplitude ($\varepsilon_1^{\text{ampl}} = 1 \cdot 10^{-2}$): a,b) Hypoplasticity with intergranular strain, c,d) ISA, e,f) Sanisand

Description	Sanisand	Hypoplasticity	ISA
Oedometric first loading	+	+++	+++
Oedometric cycles	++	+	++
Maximum stress ratio under drained conditions	+++	+++	+++
Maximum stress ratio under undrained conditions	+	++	++
Pore pressure reproduction under undrained monotonic conditions	+	++	+
Ability to avoid overshooting issues on reloading paths	++	+	++
Cyclic mobility effects	++	+	++
Accumulation rate under undrained stress controlled cycles	+	++	+
Accumulation rate under undrained strain controlled cycles	+	++	+

Table 4: Qualitative ranking of the performance of the models on different observations based on the simulations of the present work (+ + + is the best score while + is the lowest one).

Finally, a summary of the aforementioned limitations have been qualitatively ranked in Table 5.

References

[1] R.W. Boulanger and K. Ziotopoulou. Formulation of a sand plasticity plane-strain model for earthquake engineering applications. *Soil Dynamics and Earthquake Engineering*, 53:254–267, 2013.

[2] Y. Dafalias and M. Manzari. Simple plasticity sand model accounting for fabric change effects. *Journal of Engineering Mechanics*, 130(6):622–634, 2004.

[3] Y. Dafalias, A. Papadimitriou, and X. Li. Sand plasticity model accounting for inherent fabric anisotropy. *Journal of Engineering Mechanics*, 130(11):1319–1333, 2004.

[4] P. Fu and Y. Dafalias. Fabric evolution within the shear bands of granular materials and its relation to critical state theory. *International Journal For Numerical And Analytical Methods in Geomechanics*, 35(8), 2010.

[5] P. Fu and Y. Dafalias. Study of anisotropic shear strength of granular materials using DEM simulation. *International Journal For Numerical And Analytical Methods in Geomechanics*, 35(10), 2010.

[6] W. Fuentes. Contributions in mechanical modelling of fill material. Dissertation, Veröffentlichungen des Institutes für Bodenmechanik und Felsmechanik am Karlsruher Institut für Technologie, Heft 179, 2014.

[7] W. Fuentes, M. Hadzibeti, and Th. Triantafyllidis. Constitutive model for clays under the ISA framework. In Th. Triantafyllidis, editor, *Holistic simulation of geotechnical installation processes: Benchmarks and simulations*, pages 115–129. Springer International Publishing, 2016.

[8] W. Fuentes, M. Tafili, and T. Triantafyllidis. An ISA-plasticity-based model for viscous and non-viscous clays. *Acta Geotechnica*, 13(2):367–386, 2018.

[9] W. Fuentes, T. Wichtmann, and C. Lascarro. Extended hypoplasticity for sands with ISA for liquefaction analysis (submitted). *Acta Geotechnica*, 2018.

[10] I. Herle and G. Gudehus. Determination of parameters of a hypoplastic constitutive model from properties of grain assemblies. *Mechanics of Cohesive-Frictional Materials*, 4(5):461–486, 1999.

[11] X. Li and Y. Dafalias. Anisotropic critical state theory: role of fabric. *Journal of Engineering Mechanics*, 138:263–275, 2012.

[12] X. Li and X.S. Li. Micro-macro quantification of the internal structure of granular materials. *Journal of Engineering Mechanics*, 135(7):641–656, 2009.

[13] D. Masin. Incorporation of meta-stable structure into hypoplasticity. In Th. Triantafyllidis, editor, *Numerical modelling of construction processes in geotechnical engineering for urban environment*, pages 283–290. Taylor and Francis, 2006.

[14] A. Niemunis. Extended hypoplastic models for soils. Habilitation, Veröffentlichungen des Institutes für Grundbau und Bodenmechanik, Ruhr-Universität Bochum, Heft Nr. 34, 2003. available from www.pg.gda.pl/∼aniem/an-liter.html.

[15] A. Niemunis. Incremental Driver User's manual. , 2008. available from www.pg.gda.pl/∼aniem/an-liter.html.

[16] A. Niemunis and M. Cudny. Discussion on Dynamic soil-structure interaction, A three-dimensional numerical approach and its application to the Lotung case study. Poor performance of the HSS model. *Computers and Geotechnics*, 98:243–245, 2018.

[17] A. Niemunis and C.E. Grandas Tavera. Computer aided calibration, benchmarking and check-up of constitutive models for soils. Some conclusions for neohypoplasticity. In Th. Triantafyllidis, editor, *Lecture Notes in Applied and Computational Mechanics. Vol. 82. Holistic Simulation of Geotechnical Installation Processes - Theoretical Results and Applications*, pages 168–192. Springer, 2017.

[18] A. Niemunis, C.E. Grandas Tavera, and T. Wichtmann. Peak stress obliquity in drained and undrained sands. Simulations with neohypoplasticity. In Th. Triantafyllidis, editor, *Lecture Notes in Applied and Computational Mechanics. Vol. 80. Holistic Simulation of Geotechnical Installation Processes - Benchmarks and Simulations*, pages 85–114. Springer, 2015.

[19] A. Niemunis and I. Herle. Hypoplastic model for cohesionless soils with elastic strain range. *Mechanics of Cohesive-Frictional Materials*, 2(4):279–299, 1997.

[20] M. Taiebat and Y. Dafalias. SANISAND, simple anisotropic sand plasticity model. *International Journal For Numerical And Analytical Methods in Geomechanics*, 32(8):915–948, 2008.

[21] P.-A. von Wolffersdorff. A hypoplastic relation for granular materials with a predefined limit state surface. *Mechanics of Cohesive-Frictional Materials*, 1(3):251–271, 1996.

[22] D. Wegener and I. Herle. Prediction of permanent soil deformations due to cyclic shearing with a hypoplastic constitutive model. *Geotechnik*, 37(2):113–122, 2014.

[23] T. Wichtmann. www.torsten-wichtmann.de. Homepage, 2018.

[24] T. Wichtmann and Th. Triantafyllidis. An experimental data base for the development, calibration and verification of constitutive models for sand with focus to cyclic loading. Part I: Tests with monotonic loading and stress cycles. *Acta Geotechnica*, 11(4):739–761, 2016.

[25] T. Wichtmann and Th. Triantafyllidis. An experimental data base for the development, calibration and verification of constitutive models for sand with focus to cyclic loading. Part II: tests with strain cycles and combined cyclic and monotonic loading. *Acta Geotechnica*, 11(4):763–774, 2016.